Modeling and Control of a Hydraulically Actuated Flexible-Prismatic Link Robot*

Lonnie Love
Robotics and Process Systems
Oak Ridge National Laboratory
Oak Ridge, TN 37831-6426

Reid Kress
Robotics and Process Systems
Oak Ridge National Laboratory
Oak Ridge, TN 37831-6426

John Jansen
Robotics and Process Systems
Oak Ridge National Laboratory
Oak Ridge, TN 37831-6426

ABSTRACT

Most of the research related to flexible link manipulators to date has focused on single link, fixed length, single plane of vibration test beds. In addition, actuation has been predominately based upon electro-magnetic motors. Ironically, these elements are rarely found in the existing industrial long reach systems. This manuscript describes a new hydraulically actuated, long reach manipulator with a flexible prismatic link at Oak Ridge National Laboratory (ORNL). Focus is directed towards both modeling and control of hydraulic actuators as well as flexible links that have variable natural frequencies.

I. INTRODUCTION

The general philosophy behind flexible manipulators is that advanced control methods can compensate for compliance of lighter, faster, more streamlined manipulators. This manuscript describes the efforts at Oak Ridge National Laboratory (ORNL) to quantify the basic elements of industrial long reach manipulators and the effect a wide range of control strategies have on task performance. There has been a concentrated effort over the past twenty years to define new methods to control robot's with elastic links.[1,4] Unfortunately, the majority of these techniques have been tested only on single link, fixed length, single plane of vibration test beds that use electro-magnetic actuation.

A. Flexure Control Strategies

Book showed the fundamental limitation of conventional control strategies when used on flexible manipulators. He showed that the bandwidth that could be achieved by a simple PD joint controller was limited to approximately 1/3 of the clamped joint natural frequency.[2] This became a useful rule of thumb for design. Bandwidth exceeding the clamped joint natural frequency became a worthy goal.[4] Of equal interest is the tracking performance of the tip of the robot. Joint

level controls are generally sufficient for rigid manipulators. However, when there is compliance in the link, joint measurements alone may be insufficient for estimating the tip position. For this reason, many researchers have looked beyond joint sensors to more sophisticated means of measuring or estimating the robot's tip position. One of the more popular methods of measuring link deformation consists of using strain gages distributed along the length of the link. Unfortunately, the varying length of a prismatic link makes this measurement, as well as computation, impractical. Another popular form of measuring tip vibration is to use an accelerometer. Lew showed that a smaller, high bandwidth robot located on the tip of a flexible robot could use tip acceleration feedback to damp any residual vibration.[7] However, if tip position control is desired, sensor noise corrupts the extrapolation of this measurement to a deformation measurement.

There have been other methods of measuring the tip deformation or position of the flexible robot that can be easily transformed to systems with prismatic joints. However, the noncollocated actuators and sensors increase the tracking performance but limit the achievable bandwidth.[15] Wang and Vidyasagar used lateral effect photo diodes to measure link deformation. To accommodate for the nonminimum phase zeros (and subsequently the unstable controller when the plant is inverted), they proposed using positive deformation feedback in their controller.[18] This technique provides a passive controller that ensures stability while compensating for link vibration and deformation. Their results are encouraging and will be attempted in the near future on the ORNL test bed.

Another approach to vibration suppression consists of filtering, or shaping, the trajectory or command to the robot's joint controller such that the joint commands do not excite the natural modes of the elastic links. These techniques are based upon posicast control where upon a portion of an input signal is delayed by one-half of the plant's oscillation frequency to cancel induced vibration.[16] Singer and Seering first used this philosophy on flexible link robots and developed constraint relationships to improve robustness to

DISCLAIMER

parameter uncertainty.[13] Magee and Book[10], as well as Singhose, Singer, and Seering[14], have shown how to reduce the delay time, and subsequently the phase lag, of these filters. While the benefit of these filters is well understood, their performance when the plant varies dramatically, as expected with the prismatic joint, has yet to be explored. This manuscript focuses on both the control of hydraulic drives as well as flexible prismatic links. Section II describes our test bed and provides the basic modeling of hydraulic drives. The goal is to establish satisfactory joint level tracking performance and investigate flexure control strategies for the flexible-prismatic link. Section III covers the basic energy model of the prismatic link and illustrates the possible variation in link resonant frequencies. Finally, sections IV provides preliminary experimental results.

II. FLEXIBLE PRISMATIC TESTBED

One of the milestones of the research related to this test bed is to establish a feasibility study of many flexure control algorithms on an industrial sized test bed. In particular, the authors wish to explore many of the classic flexure control techniques described in the literature and establish the limitations of the methods when applied to a standard industrial type system. In many industrial applications where a high power capacity is desired, hydraulics is the preferred form of actuation. Hydraulics provide a number of unique features. First, the fluid provides a natural method of lubrication and cooling. Furthermore, hydraulic actuators have a high stiffness compared to other drive devices. In addition, they have a higher speed of response as well as large torque to inertia ratios, providing high acceleration capacity. However, hydraulics are not as linear and flexible as electromechanical devices in the manipulation of low power systems.[11] These tradeoffs provide a rich field of research that has yet to be explored. To further this research, ORNL has constructed the flexible prismatic test bed shown in Figure 1.
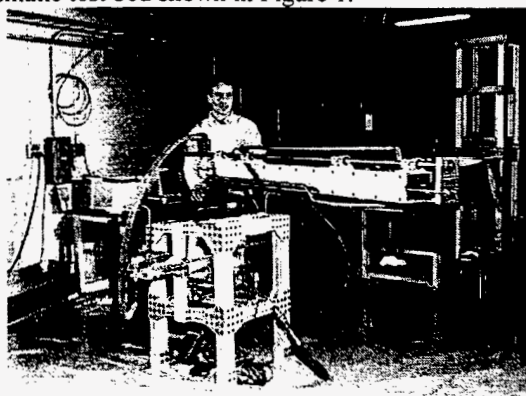

Figure 1: Flexible Prismatic Test Bed

The ORNL test bed has orthogonal rotary and prismatic degrees of freedom. The rotary actuator on the is a Parker HTR30 hydraulic rack and pinion rotary actuator. At 2000 psi, this actuator has a maximum torque capacity of 20,000 in-lb. The prismatic joint is powered by a Parker Series EH hydraulic cylinder with a 2 inch bore. Its force capacity at 2000 psi is 6280 lbf. Moog 760 series valves control the fluid flow. Both joints have position feedback as well as supply and return pressure transducers. Temperature sensors are located in the reservoir and the supply and return ports of the servovalves. Equation (1) describes the relationship between the valve opening, x_v, and the velocity, $\dot{x}_p$, of the piston.[11] Cylinder dependent characteristics include the cross sectional area, A_p, mass, M_t, portions of the total flow-pressure coefficient, K_{ce} and viscous friction, B_p of the piston and load.

$$\frac{\dot{x}_p}{x_v} = \frac{\dfrac{K_q}{A_p}}{\dfrac{V_t M_t}{4\beta_e A_p^2} s^2 + \left(\dfrac{K_{ce} M_t}{A_p^2} + \dfrac{B_p V_t}{4\beta_e A_p^2}\right)s + \left(1 + \dfrac{B_p K_{ce}}{A_p^2}\right)} \quad (1)$$

V_t represents the total volume of the fluid and β_e the effective bulk modulus of the fluid. This transfer function model is for a fixed/rigid mass load. One of the more challenging problems related to hydraulics is the nonlinear and time varying nature of the plant. Nonlinearities include high levels of stiction and coulomb friction. The valve provides many nonlinearities such as the relationship between the valve opening and flow and saturation. Furthermore, the compliance of the hydraulic fluid is temperature dependent. As the system warms up, the plant dynamics, as illustrated shortly, can vary dramatically. Subsequently, the design of a closed loop control robust to each of these characteristics can be quite tedious. Hydraulic drives are sensitive to temperature variations. Figure 2 illustrates the variation the supply and reservoir oil temperature over five hours of continuous operation. The ripple in the supply temperature is due to the dissipation of heat in the oil through the rubber hoses during high frequency operations (which require lower amounts of fluid flow). The initial increase in the reservoir temperature is due to the dominant energy in the reservoir pump. This is soon surpassed by the energy produced by the hydraulic cylinder. The oil, Houghto-Safe 620, is water-glycol based and has a bulk modulus that is sensitive to temperature variations. Figure 3 illustrates the effect of the temperature variation on the plant dynamics over the time of operation. The dominant effect is in the DC gain of the plant. As the fluid temperature rises, the effective bulk modulus of the fluid decreases. This decrease in bulk modulus directly reduces the effective stiffness of the fluid.
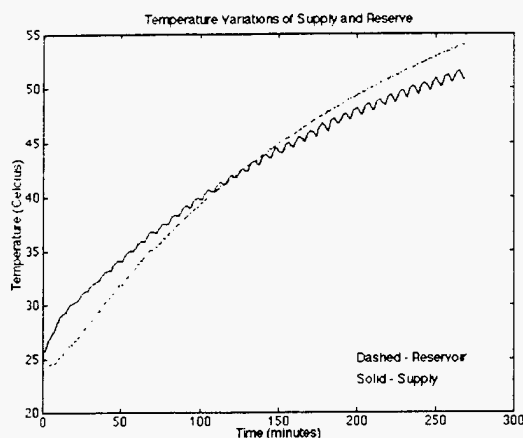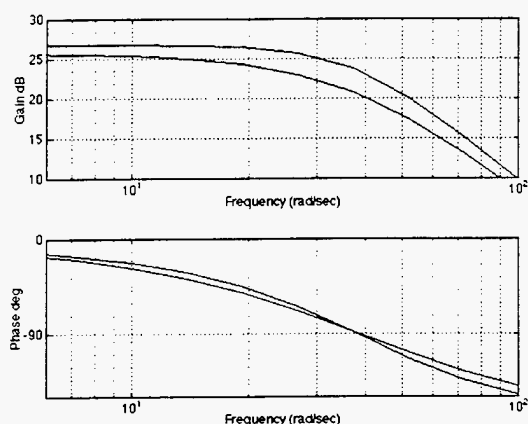
Figure 2: Temperature Variation vs. Time

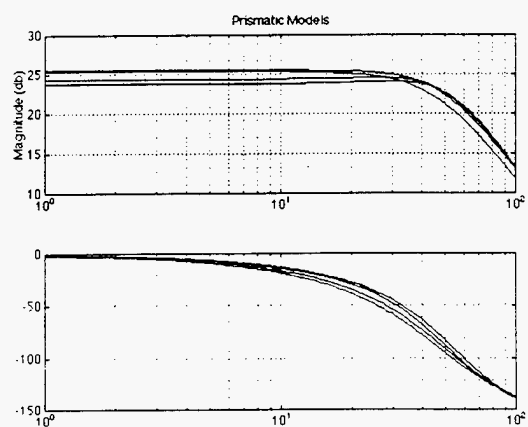**Figure 3:** Bounds on Plant Dynamics

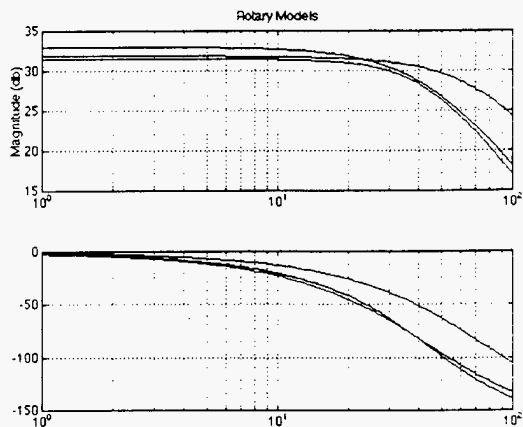**Figure 4:** Amplitude Sensitivity on Prismatic Joint

Figure 5: Amplitude Sensitivity on Rotary Joint

Figures 4 and 5 illustrate the effect of different magnitudes of input commands on the frequency response of a system. The input command ranged from 100 mV to 1 V. This produces a magnitude and phase shift up to 8 dB and 30 degrees. The selection of a joint controller must be robust to these variations. Furthermore, for the flexure control described shortly, a controller is sought that will reject potential disturbances generated by the vibration of the beam. Our strategy is to observe the effects of nonlinear and time varying phenomenon on the plant and design a series of lag-lead filters that provide high stiffness while providing sufficient gain and phase margin in the regions where nonlinearities are predominant.

A. Nonlinearities and Limit Cycle Characterization

Hydraulic systems contain many nonlinearities including nonlinear friction (both stiction and Coulomb friction), nonlinear drive-train compliance, actuator saturation, mechanical backlash and deadband, servovalve nonlinear friction and deadband, entrapped air within the hydraulic fluid, nonlinear servovalve orifice effect, the effects of fluid contamination, pressure losses from turbulent flow, fluid sensitivity to temperature changes, and time-varying nonlinear effects. These nonlinearities can introduce limit cycles during operation. A classic study of limit cycles with respect to robotics was done by Luh[9] and a recent example relative to hydraulic robots is given in Mougenet and Hayward.[12] When the flexible prismatic test bed was operated, a stable limit cycle was observed in the rotary joint at a frequency of approximately 5 Hz. Based on our past experience with many hydraulic manipulator systems[6] it was felt that the limit cycle was a result of nonlinear friction (stiction plus Coulomb) coupled with

drive-train compliance resulting from the hydraulic lines and the compressible fluid. Describing function techniques were used to analyze this nonlinearity because it was felt that the filter hypothesis held for this system (i.e. the limit cycle response was dominated by the first fundamental mode). The describing function for nonlinear friction coupled with drive-train compliance is given in Merritt's book[11] for an input of $M\sin\omega t$:

$$G_d = \frac{b_1}{M} + i\frac{a_1}{M} \qquad (2)$$

where the real and imaginary parts are calculated from

$$\frac{\pi a_1}{M} = 4\left(\frac{H_c}{M}\right)^2\left(1 + \frac{H_s}{H_c}\right) - 4\frac{H_c}{M} - \left(\frac{H_c}{M}\right)^2\left(1 + \frac{H_s}{H_c}\right)^2 \qquad (3a)$$

$$\frac{\pi b_1}{M} = \frac{\pi}{2} + \sin^{-1}\left[1 - \frac{H_c}{M}\left(1 + \frac{H_s}{H_c}\right)\right] + \qquad (3b)$$

$$\left[1 - \frac{H_c}{M}\left(3 - \frac{H_s}{H_c}\right)\right]\left[\frac{2H_c}{M}\left(1 + \frac{H_s}{H_c}\right) - \left(\frac{H_c}{M}\right)^2\left(1 + \frac{H_s}{H_c}\right)^2\right]^{1/2}$$

for stiction magnitude H_S and Coulomb magnitude H_c. To theoretically determine the existence and subsequent frequency of the limit cycle one can look for the intersection of the system transfer function with the plot of $-1/G_d$ on a Nyquist plot. Equation 4 is the transfer function model of the rotary joint

$$G_{Rotary}(s) = \frac{240810}{s(s^2 + 140s + 6150)} , \qquad (4)$$

which can be modified to account for major temperature variations by changing the numerator by plus and minus 20%. Figure 6 shows the Nyquist plot of the three different rotary joint plant models representing the nominal plant described by the transfer function of Eq. 4 and plants having plus and minus 20% variation in gain intersecting with the describing function plot for the friction coupled with drive-train compliance nonlinearity of Eq. 2 for 0%, 10%, and 20% stiction levels (i.e. stiction levels above the Coulomb values represented by H_S/H_c = 1, 1.1, 1.2, respectively).
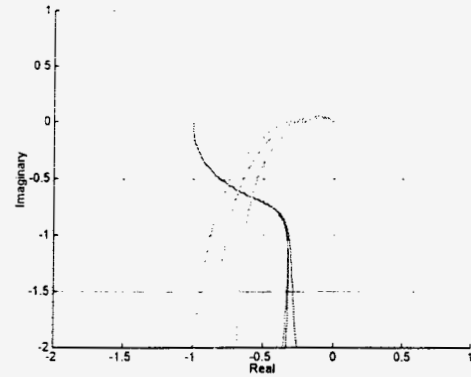

Figure 6: Nyquist plot of rotary-joint transfer functions

The gain of the nominal plant of Eq. 4 was varied by plus and minus 20% to account for uncertainty in the variation of the fluid properties such as bulk modulus.[5] Limit cycles are evident from the intersection points shown on Figure 6. These points represent frequencies in the range of 5 to 6 Hz which verifies the experimentally observed limit cycle phenomenon. Because of the form of the nonlinearity (i.e. the curves eventually intersect the $-j\omega$ axis), limit cycles cannot be completely avoided. However, compensators can be designed so that the magnitude and frequency of the limit cycles are reduced to levels that are inconsequential. Design of appropriate compensators to shape the plant response to place the limit cycle in a desired location will be the topic of future investigations.

III. DYNAMICS OF PRISMATIC DEGREE OF FREEDOM WITH COMPLIANCE

The previous sections describe many issues related to the modeling and control of hydraulic actuators. Now we must investigate what effect link compliance in a prismatic joint has on the dynamics of the robot. A number of researchers have worked on modeling a single degree of freedom flexible manipulator vibrating in a single plane.[8,17] Book, in the early 80's, investigated the dynamics of a multi-link flexible manipulators.[3] However, almost all work to date has focused on fixed link, rotary joint manipulators. A challenging problem is the control of a prismatic joint that moves a flexible link. This configuration can provide a wide range of natural frequencies, as will be illustrated shortly.

The prismatic joint consists of a hardened steel tube, one inch outer diameter with a 0.6 inch inner diameter, and can extend from twelve to sixty inches with a maximum payload capacity of seventy five pounds. With this range of payload and displacement, the arm can match the natural frequencies expected with the many

industrial long reach manipulators. With the speed capacity of the prismatic and rotary joints, it is evident that the natural frequency of the arm can vary by a magnitude over a very short range of motion.

Figure 7: Model of Flexible-Prismatic System

Figure 7 illustrates a simplified model of the flexible-prismatic test bed. The position of the link is defined in Eq. 5. This is a standard notation used for fixed link flexible manipulators.

$$\dot{r} = x\,\bar{i} + u(x,t)\,\bar{j} \qquad (5)$$

The velocity of an element in the beam includes the rotary, q_r, as well as the prismatic, q_p, motion.

$$\bar{v} = (\dot{q}_p - u(x,t)\dot{q}_r)\,\bar{i} + (\dot{u}(x,t) + x\dot{q}_r)\,\bar{j} \qquad (6)$$

Equations 7 through 9 lists the resulting kinetic and potential energy, as well as the work done by the actuators.

$$T = \frac{1}{2}\int_0^{q_p}\rho A\left[\begin{array}{l}\dot{q}_p^2 + \left(u(x,t)^2 + x^2\right)\dot{q}_r^2 + \dot{u}(x,t)^2 \\ + 2x\,\dot{u}(x,t)\dot{q}_r - 2u(x,t)\dot{q}_p\dot{q}_r\end{array}\right]dx$$

$$+ \frac{1}{2}M_t\left[\begin{array}{l}\dot{q}_p^2 + \left(u(q_p,t)^2 + q_p^2\right)\dot{q}_r^2 + \dot{u}(q_p,t)^2 \\ + 2q_p\,\dot{u}(q_p,t)\dot{q}_r - 2u(q_p,t)\dot{q}_p\dot{q}_r\end{array}\right] \qquad (7)$$

$$V = \frac{1}{2}\int_0^{q_p} E\,I\left(u''(x,t)\right)'\left(u''(x,t)\right)dx \qquad (8)$$

$$W = \tau q_r + F_p\,q_p \qquad (9)$$

Assuming that the deformation holds to the separation of variables, the displacement field, $u(x,t)$, can be replaced by a position and time dependent variable.

$$u(x,t) = \phi(x)\,q(t) \qquad (10)$$

We can now use any number of techniques to establish the dynamic equations of motion. If the displacement field has N generalized modes, there will be a total of N+2 equations of motion; one for the prismatic joint, one

for the rotary joint, and N for the generalized coordinates of the beam. One interesting twist to the derivation of the dynamics with the prismatic joint is that the limit of integration is one of the generalized coordinates. This has the effect of adding a nonlinear stiffness term to the prismatic degree of freedom.

$$\left(\rho A q_p + M_t\right)\ddot{q}_p + \left(-M_t\,\phi(q_p)q - \int_0^{q_p}\rho A\phi(x)q\,dx\right)\ddot{q}_r + \qquad (11)$$

$$\left(-M_t\,\phi(q_p) - \int_0^{q_p}\rho A\phi(x)\,dx\right)\dot{q}\dot{q}_r + \rho A\dot{q}_r^2 - \rho A\phi(q_p)q\dot{q}_p\dot{q}_r$$

$$+ \frac{1}{2}E\,I\,q'\phi'''(q_p)\,\phi''(q_p)q = F_p$$

Likewise, the rotary and generalized coordinated equations of motion are listed in Eq. 12 and 13.

$$\left[M_t q_p^2 + \frac{1}{3}\rho A\,q_p^3 + q'\left(\begin{array}{l}-M_t\phi'(q_p)\phi(q_p) - \\ \int_0^{q_p}\rho A\phi'(x)\phi(x)\,dx\end{array}\right)q\right]\ddot{q}_r +$$

$$\left(-M_t\,\phi(q_p) - \int_0^{q_p}\rho A\phi(x)\,dx\right)q\ddot{q}_p + \left[\begin{array}{l}M_t\,q_p + \frac{3}{2}\rho A\,q_p^2 + \\ \rho A\,q'\phi'(q_p)\phi(q_p)q\end{array}\right]\dot{q}_p\dot{q}_r - \qquad (12)$$

$$q'\left(-M_t\phi'(q_p)\phi(q_p) - \int_0^{q_p}\rho A\phi'(x)\phi(x)\,dx\right)\dot{q}\dot{q}_r - \rho A q_p\phi(q_p)\dot{q}\dot{q}_r$$

$$- \rho A\phi(q_p)q\dot{q}_r^2 = \tau_r$$

$$\left(M_t\phi(q_p)q_p + \int_0^{q_p}\rho A\,x\phi(x)dx\right)\ddot{q}_r + \left(\begin{array}{l}M_t\phi'(q_p)\phi(q_p) + \\ \int_0^{q_p}\rho A\phi'(x)\phi(x)dx\end{array}\right)\ddot{q} +$$

$$\rho A\phi'(q_p)\phi(q_p)\dot{q}_p\dot{q} + \left(\begin{array}{l}\rho A q_p\phi(q_p) + M_t\phi(q_p)) \\ + \int_0^{q_p}\rho A\phi(x)dx\end{array}\right)\dot{q}_p\dot{q}_r$$

$$+ \left(\int_0^{q_p}E I\phi'''(x)\phi''(x)dx\right)q = 0 \qquad (13)$$

This model can now be transformed to the standard state space representation. To illustrate the influence of the prismatic joint on the systems dynamics, Figure 8 shows the variation in the link's natural frequency as a function of its displacement and payload.
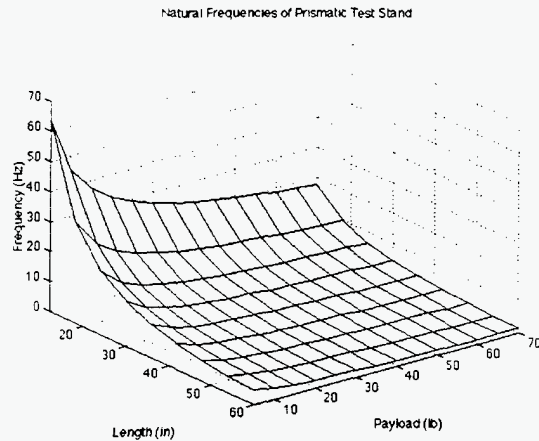
Figure 8: Payload and Position Dep. Natural Freq.

IV. EXPERIMENTAL RESULTS

The final series of experiments conducted in this investigation focused on comparing both filtering and passive end point feedback control for vibration suppression. Two popular filtering methods are compared first. These include the robust notch filter and the three term input shaping filter. Focal frequencies included initial and final configurations. A third adaptive filtering scheme is introduced. This filter, based on the three term shaping filter, varies the filter frequency with an estimate of the beam natural frequency. The experiment consists of executing a straight line maneuver. The path, using a minimum time trajectory, consists of moving 30 inches in the positive X direction, holding for 2 seconds, moving in the negative X direction 60 inches, holding for 2 seconds, then moving back 30 inches in the positive X direction. The path has a maximum acceleration of 100 in/sec^2 and velocity of 10 in/sec. The arm had a payload of 45 pounds during the duration of the maneuver. Without any flexure compensation, there is considerable vibration in the arm, evident in Figure 9.
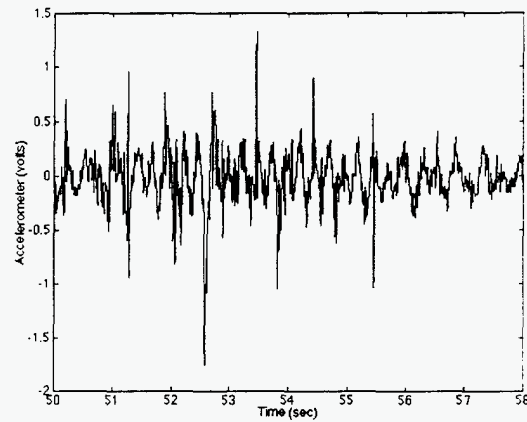

Figure 9: Tip Acceleration, No Flexure Control

To demonstrate the performance of simple filtering techniques, a basic three term input shaping filter derived by Magee[10], was implemented on the rotary joint of the robot.

$$F(z) = \frac{1 - 2\cos(\omega_d T)\, e^{-\zeta \omega_n T} e^{-sT} + e^{2\zeta \omega_n T} e^{-2sT}}{1 - 2\cos(\omega_d T)\, e^{-\zeta \omega_n T} + e^{2\zeta \omega_n T}} \qquad (14)$$

Figure 10 illustrates the resulting response of the system during the same maneuver. A comparison of the frequency response shows approximately a 20 db improvement in the magnitude of vibration. (Note that acceleration measures the product of ω^2 and amplitude but considering a ratio of acceleration levels at the same frequency cancels the ω^2 term.)
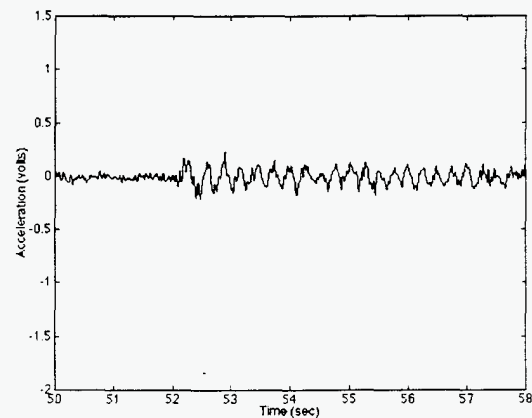

Figure 10: Tip Acceleration with Filter

VI. CONCLUSIONS

The advantage of long reach manipulators has been discussed for over twenty years. There is a growing

desire to push this research into field applications. Research at ORNL is focusing on advanced control techniques for both hydraulic actuation and flexure control. The advantage of hydraulic systems is their high payload-to-weight ratio over electric, their bandwidth, and their high power capacity. However, as shown in this manuscript, there are many nonlinear and time varying characteristics that complicate control design. The approach outlined in this manuscript consists of first identifying the effect of each of these nonlinearities in the frequency domain. Once these characteristics are understood, linear controllers are designed, using simple lag-lead filters, that attempt to maximize the stiffness of the actuators while providing sufficient gain and phase margin to ensure robust stability. Next, focus shifted towards the effect of variable length link compliance. Preliminary experiments show that marginal improvement is possible using simple input shaping filters. Work is presently under way to compare adaptive filters as well as link deformation feedback, but was not complete at the time of this submission.

REFERENCES

1. Book, W, Whitney, D., and Lynch, P., "Design and Control Considerations for Industrial and Space Manipulators," *Proceedings of The Joint Automatic Control Conference*, Austin, TX, 1974, pp. 591-598.

2. Book, W., Maizzo-Neto, O., and Whitney, D., 1975, "Feedback Control of Two Beam, Two Joint Systems with Distributed Flexiblity," *ASME Journal of Dynamic Systems, Measurement, and Control*, Vol.97, pp.424-431.

3. Book, W., "Recursive Lagrangian Dynamics of Flexible Manipulator Arms," *The International Journal of Robotics Research*, Vol. 3, pp.87-101.

4. Book, W., "Controlled Motion in an Elastic World," *ASME Journal of Dynamic Systems, Measurement, and Control*, June 1993, Vol.115, No.2B, pp.252-261.

5. Jinghong, Y., Zhaoneng, C., and Yuanzhang, L., "The Variation of Oil Effective Bulk Modulus with Pressure in Hydraulic Systems," *ASME Journal of Dynamic Systems, Measurement, and Control*, Vol. 116, No.1, March 1994, pp.146-150.

6. Kress, R. L., Jansen, J. F., Love, L. J., and Basher, A. M. H., "Hydraulic Manipulator Design, Analysis, and Control at Oak Ridge National Laboratory," ORNL/TM-13300, Sep. 1996.

7. Lew, J., Trudnowski, D., Evans, M., Bennett, D., "Micro-Manipulator Motion Control to Suppress Macro-Manipulator Structural Vibrations," *Proceedings of the 1995 IEEE International Conference on Robotics and Automation*, May 1995. Vol.3, Nagoya, Japan, pp.3116-3120.

8. Low, K., "A Study of Beam Theories for Flexible Robot Manipulators," *Proceedings of the International Symposium on Robotics and Automation*, May, 1989.

9. Luh, J. Y. S. and Paul, R. P. C., "Joint Torque Control by a Direct Feedback for Industrial Robots," *IEEE Transactions on Automatic Control*, Feb. 1983, Vol. AC-28, No. 2, pp. 153-161.

10. Magee, D., and Book, W., "Filtering Micro-Manipulator Wrist Commands to Prevent Flexible Base Motion," *Proceedings of the American Control Conference*, June 1996, pp.924-928.

11. Merritt, H., Hydraulic Conrol Systems, John Wiley & Sons, 1967.

12. Mougenet, F. and Hayward, V., "Limit Cycle Characterization, Existence and Quenching in the Control of a High Performance Hydraulic Actuator," *Proceedings of the IEEE International Conference on Robotics and Automation*, May 1995, Vol.3, Nagoya, Japan, pp.2218-2223.

13. Singer, N., and Seering, W., "Preshaping Command Inputs to Reduce System Vibration," *ASME Journal of Dynamic Systems, Measurement, and Control*, March 1990, Vol. 112, No.1, pp.76-82.

14. Singhose, W., Singer, N., and Seering, W., "Design and Implementation of Time-Optimal Negative Input Shapers," *1994 ASME IMECE*, DSC-Vol.55-1, Dynamic Systems and Control: Vol.1, pp.151-157.

15. Spector,V., and Flashner,H., 1990, "Modeling and Design Implications of Noncollocated Control in Flexible Systems," *ASME Journal of Dynamic Systems, Measurement, and Control*, June 1990, Vol.112, pp.186-193.

16. Tallman, G., and Smith, O., "Analog Study of Dead-Beat Posicast Control," *IRE Transactions on Automatic Control*, March 1958, Vol.PGAC, No.4, pp.14-21.

17. Usoro,P., Nadira,R., Mahil.S., "A Finite Element/Lagrange Approach to Modeling Lightweight Flexible Manipulators," *ASME Journal of Dynamic Systems, Measurement, and Control*, Vol. 108, pp.198-205.

18. Wang, D., and Vidyasagar, M., "Transfer Functions for a Single Flexible Link," *International Journal of Robotics Research*, Oct. 1991, Vol. 10, No. 5, pp.540-549.

Report Number (14) _ORNL/CP-96159_
CONF-970469 --

Publ. Date (11) _199612_
Sponsor Code (18) _DOE, XF_
JC Category (19) _UC-900, DOE/ER_

DOE